Horizontal Entrainment and Detrainment in Large-Scale Eddies

MELVIN E. STERN*

Graduate School of Oceanography, University of Rhode Island, Narragansett, RI 02882

(Manuscript received 3 October 1986, in final form 28 April 1987)

ABSTRACT

We compute the evolution of disturbances on a circularly symmetric eddy having uniform vorticity in a central core, in a surrounding annulus, and in the irrotational exterior water mass. This vortex is known to be (Kelvin–Helmholtz) unstable when its annular width is less than the core radius. Our calculations for the nonlinear regime show that amplification of azimuthal wavenumber $n = 2$ causes the vortex to split into two dipoles, in agreement with previous numerical calculations for a smoothed version of our vorticity field. This paper concentrates on the evolution of large-amplitude disturbances on the outer edge of a stable and robust eddy. We show that lateral wave breaking of vorticity isopleths causes intrusions of the (irrotational) exterior water mass into the central core of the vortex, a physical process which is relevant to lateral diffusion and isopycnal mixing in baroclinic ocean eddies. Similar intrusive features occur for an $n = 1$ disturbance, which also causes a "self-propagation" of the entire eddy. The large-amplitude disturbances on the eddy can be initiated by the action of external eddies or currents. A simple model for this case exhibits filaments detraining from the eddy, as well as intrusive features.

1. Introduction

The thin filamentary streamers extending outward from the edge of warm core rings are familiar features of the surface temperature, as revealed by satellite images. Additional hydrographic measurements at greater depths (Cheney and Richardson, 1976; Lambert, 1984; Joyce, 1984; Joyce et al., 1983; Schmitt et al., 1986) suggest that such outward-going filaments, and also the inward-coming intrusions, are important links from the geostrophic scale to the smaller scales (fine structure) responsible for the dissipation of the salinity–temperature variances which are continually generated by evaporation and solar heating. This paper addresses the mechanism of the lateral diffusion process which starts from the geostrophic scale.

Although warm/cold core eddies originate as instabilities of current systems separating different water masses, these coherent and long-lived vortices are robust. Their outer boundary, however, is continually deformed by the ambient motion field, and by topographic or *beta* effects. We suggest that these large-amplitude deformations produce folding or "wave breaking" of potential vorticity isopleths, followed by either intrusions of the surrounding water or by "detrainment" of long, thin filaments into the surrounding water mass. Stern (1987) has shown how these features can "pinch off" in a "1½-layer" density model of a disturbed rectilinear current. This paper considers the analogous effects in a round barotropic model, and we believe the main qualitative effect will also occur in a baroclinic vortex.

The model is simplified even further by assuming that the vortex has piecewise uniform vorticity. This leads to a reduction in the number of spatial dimensions, so that the resulting mathematical problem is focused entirely on the evolution of the interfaces between the vorticity domains. The highly filamented structures appearing in this calculation are easily resolved, reproduced, and rationalized.

The large amount of literature on this "contour dynamical" technique (Melander et al., 1986) has mainly been applied to noncompact eddies, each having finite far-field circulation (and infinite kinetic energy). The more relevant oceanographic structure seems to be a *compact* structure, such as a vortex having vanishing far-field circulation, but the mathematical apparatus is the same. We also mention that some of the previous calculations compare favorably with two-dimensional calculations of high resolution for *smoothed* vorticity fields, and this observation produces confidence in the thin filamentary vorticity structures which we shall obtain for the piecewise uniform models.

In section 2 we start with the problem of the stability of a piecewise uniform vorticity eddy (Flierl, 1985). This problem is the "round" version of the elementary Kelvin–Helmholtz problem, and from the calculation outlined in section 2 it is found that the compact vortex is stable if the ratio of the radii of the outer and inner interfaces is $a > 2$. For a slightly smaller ratio, only azimuthal wavenumber $n = 2$ amplifies with time. The

* Present affiliation: Dept. of Oceanography, Florida State University, Tallahassee, FL 32306.

normal mode for $n = 1$ has an interesting degeneracy (with frequencies: $\sigma^2 = 0$), the resolution of which (section 2) shows that an *initial* $n = 1$ disturbance results in the self-propagation of the entire vortex with constant speed and direction. Next we turn to the nonlinear phase of an unstable vortex. For the case of *smooth* vorticity field, Gent and McWilliams (1986) have shown the splitting into two dipole eddies, which then propagate away from each other. (Ikeda, 1981, obtained a similar effect for a baroclinic vortex which was barotropically stable.) The effect is reproduced (section 3) in the piecewise uniform vorticity model, and we also show that dipolar splitting occurs no matter how small: $2 - a > 0$.

Our main interest, however, is the linearly stable eddy ($a > 2$) subjected to large-amplitude initial deformations at its outer boundary. In this case the finite miminum width of the annular region can decrease to zero as time increases. This effect causes a thin filament of the exterior (irrotational) water mass to spiral inwards towards the radius of maximum azimuthal velocity. (If the uniform density field in our model was composed of compensating temperature and salinity fields, then we would see lateral intrusions of these fields.)

The question then arises as to the mechanism by which the large-amplitude initial perturbations are generated. In section 5 we put a single fixed point vortex at varying distances outside a circularly symmetric eddy, and then compute the evolution of the disturbances forced on the outer boundary. The numerical solutions of the contour dynamical equations reveal detraining filaments as well as ingoing intrusions.

2. Analytical considerations

a. *Small perturbation theory*

Consider the undisturbed eddy whose azimuthal velocity is

$$\bar{u}(r) = \begin{cases} r, & 0 \leqslant r \leqslant 1 \\ -r/(a^2-1) + a^2/r(a^2-1), & 1 \leqslant r \leqslant a \\ 0, & r > a. \end{cases} \quad (1)$$

The maximum (nondimensional) velocity is unity, the radius of the inner core is unity, and the vorticity of the latter is +2. In the annulus the value of $\bar{u}$ decreases to zero at the outer interface, and the vorticity of the annulus is

$$w = -2/(a^2-1). \quad (1a)$$

Figure 1 depicts the two interfaces for a particular initial state in which the centers of the two circles are displaced from each other by an amount Δ.

Since the vorticity is piecewise uniform, the conservation law will be satisfied if the perturbation is piecewise irrotational. Let us begin by making a normal mode *ansatz*, so that the streamfunction is assumed to be given by the real part of

$$\hat{\psi}(r)e^{in\theta+\sigma t}$$

where n is the wavenumber, σ is the frequency, and $\hat{\psi}$ is the eigenfunction of the mode. But let us bear in mind that normal modes are not necessarily complete and are not necessarily capable of describing the evolution of *all* initial perturbations.

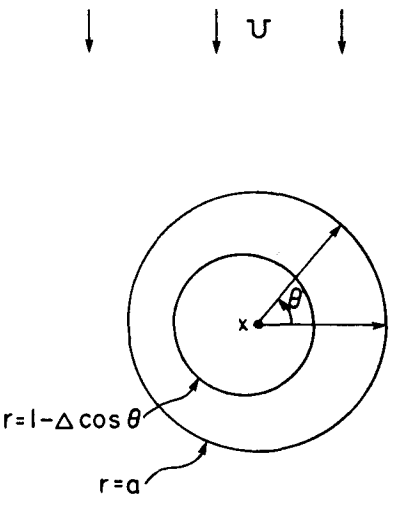

FIG. 1. An example of a piecewise uniform vorticity eddy, in which the center of the outer circle ($r = a$) is displaced from the center of the inner one (marked ×) by an amount Δ. If $\Delta \ll 1$, the entire vortex propagates upwards with speed U, and the diagram shows the relative motion in a polar coordinate system fixed to the center of the outer circle.

The solution of Laplace's equation shows that $\hat{\psi}$ is a linear combination of $r^{\pm n}$ in each of the three pieces of the eddy. The combination must be regular at $r = (0, \infty)$, and the pieces must be connected across $r = (1, a)$ so that $\hat{\psi}(r)$ and the azimuthal pressure gradient (or the perturbation in azimuthal acceleration) are continuous. It can be shown that the latter requirement at the inner interface implies

$$(1-\sigma)[\hat{\psi}'(1+) - \hat{\psi}'(1-)] + \frac{2a^2}{a^2-1}\hat{\psi}(1) = 0 \quad (1b)$$

where the prime denotes a derivative with respect to r, and a similar connection condition for the streamfunction at $r = a$ can be obtained. One then substitutes the piecewise irrotational $\hat{\psi}$ into these, thereby obtaining the dispersion equation

$$n^2\sigma^2 + \sigma(n-n^2) + \frac{n + a^2(a^{-2n}-1)(a^2-1)^{-1}}{a^2-1} = 0. \quad (2)$$

The two σ-roots are real for all n if $a \geqslant 2$, and at $a = 2$ the $n = 2$ mode is on the verge of amplification. The real part of its frequency is $\sigma = \frac{1}{4}$, and the radial displacements of the perturbed interfaces are equal and opposite.

A normal mode with $n = 1$ does not change the shape of the circular interfaces to first order in amplitude, but only displaces their centers. Note that if $n = 1$ in Eq. (2), then $\sigma^2 = 0$. One of these two degenerate eigenvalues corresponds to a trivial disturbance, in which each of the two circular interfaces is displaced by the *same* amount from the origin of a fixed coordinate system. Of course nothing will happen ($\sigma = 0$) in this case, but if the displacements differ by Δ (Fig. 1), then the $n = 1$ initial perturbation is obviously nontrivial and nonstationary. The paradox ($\sigma^2 = 0$) is due to the incompleteness of the normal modes.

The Δ displacement in Fig. 1 can be interpreted as a "dipole moment" of two overlapping circular domains (one with vorticity w and a larger one with vorticity $2 - w$), having equal and opposite integrated vorticities [because of (1a)]. Since the mutual induction of the domains will cause each one to move in the same direction, we shall compute the evolution of this $n = 1$ initial state by making the *ansatz* that the curves in Fig. 1 propagate without change of shape (for $\Delta \ll 1$) and with speed U. In a translating coordinate system whose center is fixed to the center of the large circle the motion is steady, and the polar equation for the inner circle is $r = 1 - \Delta \cos\theta$. For $r > a$ (Fig. 1), the total velocity is composed of the sum of U and an $n = 1$ component $\mathbf{V}(r, \theta)$. The radial component of the latter must be $\hat{v}(a, \theta) = U \sin\theta = \mathrm{Re}(-iUe^{i\theta})$ since the total radial velocity vanishes on $r = a$. Also $\hat{v}(a, \theta) = -\mathrm{Re}(ia^{-1}\hat{\psi}(a)e^{i\theta})$ if $\mathrm{Re}\ \hat{\psi}(r)e^{i\theta}$ denotes the streamfunction for the $\mathbf{V}$ component, and it then follows that $\hat{\psi}(a) = aU$. Therefore, $\hat{\psi}(r) = a^2U/r$ for $r > a$, and by adding the r derivative of this to the projection of U on the outer circle we obtain the *total* azimuthal velocity

$$u^*(a, \theta) = \mathrm{Re}(-2Ue^{i\theta}). \tag{2a}$$

Now consider $a > r > 1$, where the total velocity is given by the sum of [Eq. (1)] and an $n = 1$ component. The latter is irrotational and its radial component must vanish on $r = a$, so that the corresponding streamfunction is $F(r/a - a/r)e^{i\theta}$ where F is a constant. Since the basic velocity vanishes on $r = a$, the total azimuthal velocity is

$$u^*(a, \theta) = F\,\mathrm{Re}2a^{-1}e^{i\theta},$$

and since there can be no discontinuity in tangential velocity, Eq. (2a) implies

$$F = -aU. \tag{2b}$$

Finally, consider $0 < r < 1$, where the total field is again given by the sum of the basic velocity and an $n = 1$ perturbation. The streamfunction for the latter, which matches the previous one as $r \to 1$, is $\mathrm{Re}[rF(1/a - a)e^{i\theta}]$, and the corresponding radial velocity, evaluated at $r \to 1$, is

$$\mathrm{Re}[-iF(1/a - a)e^{i\theta}] = \mathrm{Re}[-iU(a^2 - 1)e^{i\theta}]. \tag{2c}$$

In the vicinity of the perturbed interface ($r = 1 - \Delta \times \cos\theta$) the azimuthal velocity is $\bar{u}(1) = 1$ to leading order, so that the radial velocity at $r \to 1$ must also be given by

$$\frac{\partial r}{\partial \theta} = -\mathrm{Re}i\Delta e^{i\theta}.$$

By equating this and (2c) we get

$$U = \Delta/(a^2 - 1) \tag{3}$$

as the vortex speed for a given initial $\Delta \ll 1$. It only remains to show that the azimuthal pressure gradient on either side of the $r = 1$ interface is continuous. This can be verified a posteriori by setting $\sigma = 0$ in Eq. (1b), and by substituting therein the previously obtained streamfunctions. The left-hand side of (1b) will then identially vanish, implying that the dynamical boundary condition on the inner interface is indeed satisfied. In addition to their intrinsic interest, these linear results will provide useful check and reference points for the numerical calculations in the strongly nonlinear regime.

b. Contour dynamics for large amplitudes

All the nonlinear calculations which follow are based on the method of contour dynamics (Overman and Zabusky, 1982). This method proceeds from the elementary fact that a "point" vortex at (ξ, η) with strength $qd\xi d\eta$ will produce a circularly symmetric streamfunction $(q/2\pi)\ln[(x - \xi)^2 + (y - \eta)^2]^{1/2}$ at all points (x, y). Therefore, if q is constant within a simply connected area then the Cartesian velocity components at any x, y are

$$v(x, y, t) = \frac{q}{4\pi}\frac{\partial}{\partial x}\int\int d\xi d\eta \ln(x - \xi)^2 + (y - \eta)^2$$

$$= \frac{q}{4\pi}\oint d\eta \ln(x - \xi)^2 + (y - \eta)^2$$

$$u(x, y, t) = \frac{-q}{4\pi}\frac{\partial}{\partial y}\int\int d\xi d\eta \ln(x - \xi)^2 + (y - \eta)^2$$

$$= \frac{q}{4\pi}\oint d\xi \ln(x - \xi)^2 + (y - \eta)^2$$

where the line integrals are taken counterclockwise along the curve (ξ, η) bounding the area in question. The vorticity of our doubly connected domain (an example of which is given in Fig. 1) may be considered as the sum of the vorticities in two overlapping singly connected domains, each having uniform q. The larger domain has the vorticity $q = w$ of the annulus, while the inner domain has the vorticity $q = 2 - w$, so that in the overlapping area the sum equals the actual vorticity ("two") of the core. The (principle parts of the) foregoing integrals are evaluated at each point [$x = x_2$, $y = \bar{\lambda}_2(x, t)$] on the outer boundary, and set equal to the corresponding Lagrangian velocity dx_2/dt, $d\bar{\lambda}_2/dt$. The same thing is done at a point $(x_1, \bar{\lambda}_1)$ on the inner

boundary, and in this way we obtain the coupled integro-differential equations

$$\begin{pmatrix} d\bar{\lambda}_2/dt \\ dx_2/dt \end{pmatrix} = \frac{w}{4\pi} \oint \begin{pmatrix} d\eta_2 \\ d\xi_2 \end{pmatrix} \ln(x_2-\xi_2)^2+(\bar{\lambda}_2-\eta_2)^2 + \frac{2-w}{4\pi} \oint \begin{pmatrix} d\eta_1 \\ d\xi_1 \end{pmatrix} \ln(x_2-\xi_1)^2+(\bar{\lambda}_2-\eta_1)^2$$

$$\begin{pmatrix} d\bar{\lambda}_1/dt \\ dx_1/dt \end{pmatrix} = \frac{2-w}{4\pi} \oint \begin{pmatrix} d\eta_1 \\ d\xi_1 \end{pmatrix} \ln(x_1-\xi_1)^2+(\bar{\lambda}_1-\eta_1)^2 + \frac{w}{4\pi} \oint \begin{pmatrix} d\eta_2 \\ d\xi_2 \end{pmatrix} \ln(x_1-\xi_2)^2+(\bar{\lambda}_1-\eta_2)^2$$

for the evolution of the contours $(\bar{\lambda}_1, \bar{\lambda}_2)$.

We have solved these numerically on a personal computer by placing $N(1)$ Lagrangian points on the inner boundary and $N(2)$ points on the outer one. The integrals are approximated by the trapezoidal rule with an indentation at the logarithmic singularity, whose contribution is evaluated by an analytic approximation. A second-order Runge-Kutte scheme with a time step = 0.1 was used in all the calculations reported below. When the Lagrangian points became too sparse (or too dense), we went back to a slightly earlier time and edited the output by inserting or deleting points. The calculation was then continued from this earlier time (after checking its results with those of the prior run in the overlapping region of time).

3. The unstable regime and intrusions

The numerical program was also checked by running it at the point of marginal stability ($a = 2$) with an initial condition corresponding to an $n = 2$ normal mode having a radial perturbation amplitude $\lambda_1 = -0.05$ on the inner circle and $\lambda_2 = +0.05$ on the outer circle. With $N(1) = N(2) = 80$ the phase speed differed from the linear theory ($\sigma = \frac{1}{4}$) by an amount (1%) comparable with the truncation error in evaluating the contour integrals. We then considered a stable value of $a = 2.2$, and applied an $n = 2$ initial radial disturbance ($\mathrm{Re}\lambda e^{in\theta}$) with amplitudes $\lambda_1 = -\lambda_2 = -0.2$. The counterclockwise rotation of the phase of the inner and the outer boundary (Fig. 2) reveals an evolution qualitatively similar to linear theory. This pattern is to be compared with the evolution (Fig. 3a, b) in the highly unstable regime ($a = 1.6$) where the initial condition consisted of an exact $n = 2$ normal mode with infinitesimal amplitudes $\lambda_1 = +0.05$, $\lambda_2 = (0.84) \times (0.05) \times \exp(-2.32i)$. Two different effects may be noted here, the first being the expected exponential growth which caused the minimum radius of points on the outer boundary to decrease with time. As these points are brought nearer to the inner boundary their azimuthal velocity increases, causing them to overtake the slower points on the contour at greater r, and thereby producing the incipient wavesteepening effect (Stern, 1985) at $t = 7$ in Fig. 3a. Shortly afterwards (at $t = 8$) the radial displacement of the contour becomes a multivalued function of θ ("wave breaking"). The combined effects of "growth" and "wave breaking" explains the later evolution (Fig. 3b) in which the negative vorticity is stripped away from the annulus and concentrated into two cores at the ends of the cyclonic region. The velocities induced by the anticyclonic cores will subsequently cause the cyclonic region to thin and split at its midsection, according to the longer two-dimensional calculations of Gent and McWilliams (1986), which show the ultimate split into two oppositely propagating dipoles. We mention that these calculations required a doubly periodic *array* of vortices and also a small amount of eddy viscosity, neither of which are present in the contour dynamical calculation. Figure 4 shows that the same evolution occurs even for a value of $a = 1.9$ which is only *slightly* less than the critical value. Thus *all* linearly unstable monopolar barotropic vortices will not equilibrate until there is a drastic topological change into two oppositely propagating dipoles. Since such drastic instabilities do not occur in most ocean eddies (e.g., warm/cold core rings), we turn our attention to a stable vortex ($a > 2$) subject to such large peripheral disturbances as may be initiated by surrounding eddies.

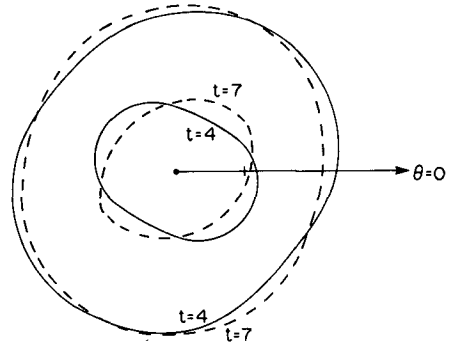

FIG. 2. Evolution of a finite amplitude $n = 2$ initial disturbance in the stable regime $a = 2.2$ with $\lambda_1 = -\lambda_2 = -0.2$. The two boundaries at $t = 4$ are drawn with a solid curve, and the $t = 7$ boundaries are drawn with a dashed curve. The tick mark on the $\theta = 0$ axis is at $r = 1$.

When the same initial disturbance [$n = 2$, $\lambda_2 = 0.2 = -\lambda_1$] as used for Fig. 2 is applied to a smaller $a = 2$, the behavior (Fig. 5a, b) is significantly different, insofar as a thin intrusion of the exterior water mass comes into close contact with the core interface (the curve of maximum circulation). When this occurs, we shall say that "intrusive instability" is exhibited. Although this also occurs in Fig. 2, there is a great difference between the two kinds of instability. The eddy in Fig. 5b is robust, ending up with nearly azimuthal velocities and a streamfunction (not shown) having a monopolar character.

Figure 6a, b shows what happens when the outer

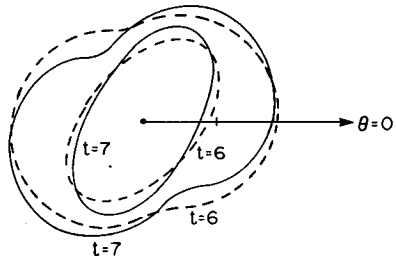

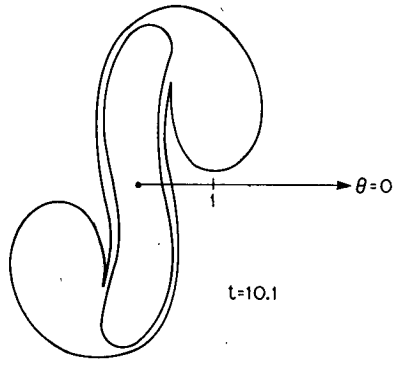

FIG. 3. Evolution of a small amplitude $n = 2$ normal mode (see text) for a highly unstable value of $a = 1.6$. (a) The number of Lagrangian points on the inner boundary is $N(1) = 80$, and $N(2) = 80$ points are on the outer boundary. The time step = 0.1. The tick mark is at $r = 1$. Wavebreaking on the outer boundary occurs shortly after $t = 7$. (b) At $t = 10.1$, two oppositely propagating dipoles start to form. The negative vorticity is concentrated in two cores at opposite ends of the elongated positive vorticity region. Prior to this time the number of Lagrangian points has been increased to $N(1) = 90$, $N(2) = 104$.

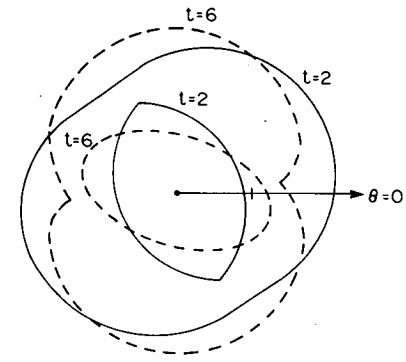

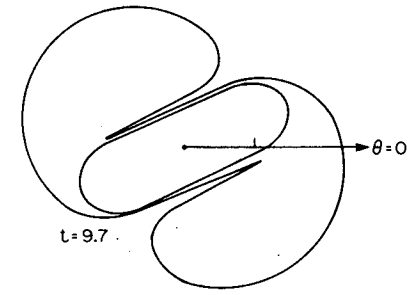

FIG. 5. As in Fig. 2 except $a = 2$. (a) Initially $N(1) = N(2) = 80$. At $t = 6$, wave breaking occurs on the outer boundary of the vortex. (b) At $t = 9.7$, the number of points on the outer boundary has been increased to $N(2) = 98$ in order to resolve the thin intrusive filaments.

radius is increased to $a = 2.3$ and the initial amplitudes of $n = 2$ are also increased to $\lambda_2 = 0.4 = -\lambda_1$. The area of the thin tip of the inner contour at $t = 3$ became so small at $t = 4.5$ that "surgery" was performed by deleting all of the points in the tip and then reconnecting the ends of the contour. At $t = 7$ (Fig. 6b) it was necessary to add points in the highly strained region of the thin intrusion, so as to maintain the spatial resolution. In the summary of Fig. 7 the symbol "S" designates those runs in which the inner boundary remains (well) separated from the outer one and from the exterior water mass. The symbol U designates ordinary instability if $a < 2$ or intrusive instability if $a > 2$.

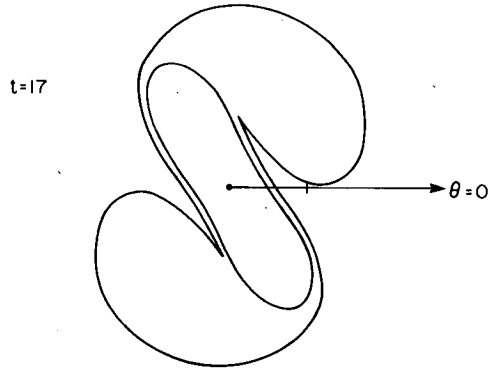

FIG. 4. As in Fig. 2 except $a = 1.9$ (slightly unstable) and $\lambda_1 = -\lambda_2 = -0.05$. Points were added at $t = 16$ so that $N(1) = 90$, $N(2) = 94$.

4. Self-propagating vortices and their intrusions

In section 2 we found that for a small relative displacement between the centers of two circular interfaces the eddy will move without change of shape and with speed (3). For large $\Delta = 1$ ($a = 2.5$), Fig. 8 shows the interfacial deformation, and the crosses in Fig. 9 show the slightly curving path of the center of gravity of the core.

Calculations were also made for an initial disturbance with azimuthal wavenumber $n = 1$, in which the interfaces are given by $r = 1$ and $r = a + \Delta \cos\theta$. For finite Δ the latter curve departs significantly from a circle, and bounds an area greater than πa^2. Therefore, its far-field circulation will be anticyclonic if (Δ, a, w) have the same values as used for the previous case of the *circular* interfaces. A comparison between the two cases is furnished by the two triangular points in Fig. 9, which indicate that the $n = 1$ mode has a slightly smaller path curvature than the corresponding case for displaced *circles*. But for $\Delta = 0.4$ the elliptical distortion of the outer boundary is so small that the path (Fig. 9) from $t = 0$ to $t = 32$ is nearly along the

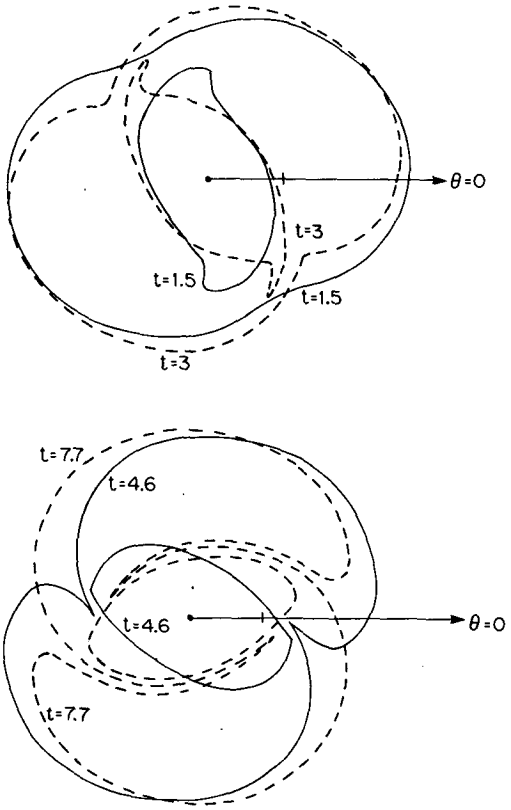

FIG. 6. As in Fig. 4 except $a = 2.3$, $\lambda_2 = 0.4 = -\lambda_1$. The tick mark on the $\theta = 0$ axis is a unit distance from the origin. (a) Notice the thin tip which forms on the inner boundary. $N(1) = N(2) = 80$. (b) "Surgery" at $t = 4.5$ has removed the tip, and at $t = 4.6$ (dashed curves), we see a filament of irrotational fluid at the inner core boundary $N(2) = 98$.

straight line predicted by the linear theory for displaced circles. Figure 9 also shows the increased curvature of the path which results when the anticyclonic vorticity

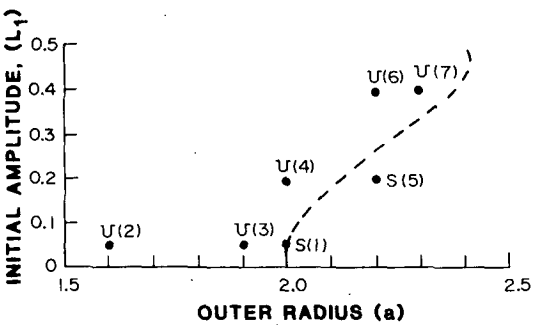

FIG. 7. Regime diagram. S indicates initial states for which the minimum width of the anticyclonic annulus does not decrease to zero. The linearly unstable regime $a < 2$ evolves into two dipoles. For the other U states the minimum width of the annulus decreases to zero, and a thin filament of irrotational fluid makes close contact with the core. The numbers in parenthesis are for identification of the run. For all runs, except run 2 (mentioned previously), the amplitude ratio was $\lambda_2/\lambda_1 = -1$ and $n = 2$.

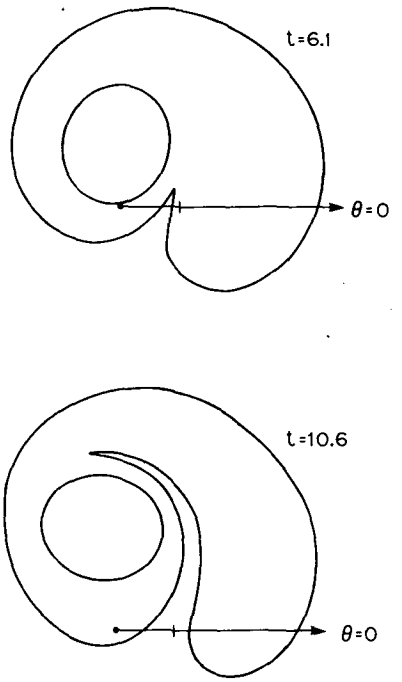

FIG. 8. The initial condition consists of two circular boundaries displaced horizontally by $\Delta = 1$, and with vanishing integrated vorticity. $N(1) = 80$, $N(2) = 100$. Note the entrainment of irrotational fluid into the central region of the eddy as it moves upward. The tick mark on the stationary $\theta = 0$ axis is at unit distance from the origin.

in the annulus is reduced relative to the constant value used in all the previous calculations. The normalized displacements of the eddy perpendicular to the initial

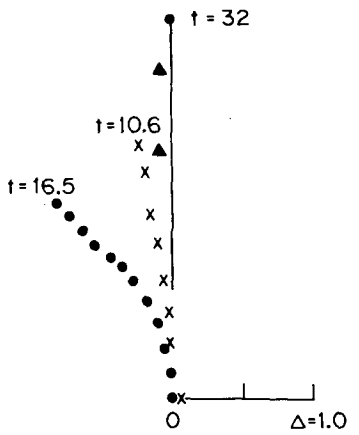

FIG. 9. The path of the center of gravity of the inner core for $a = 2.5$. The annular vorticity is the same ($w = -2/5.25$) for all points except the dotted ones ending at $t = 16.5$ (for which $w \approx -0.25$). The run with the crosses (ending at $t = 10.6$) is for an initial condition consisting of two *circles* displaced by $\Delta = 1$ (Fig. 8). The two triangular points are for an $n = 1$ initial perturbation of the outer interface with the same Δ, a, w, and these give a small excess anticyclonic vorticity to the entire annulus (see text). The straight vertical line ending at $t = 32$ indicates the path for the same a, w values but with $\Delta = 0.4$.

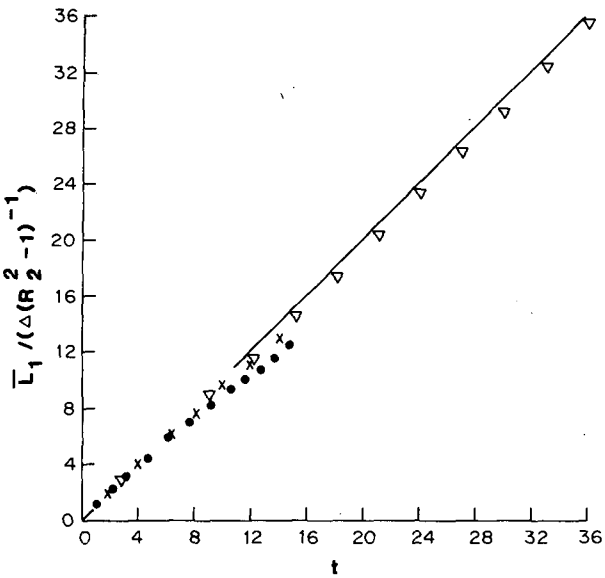

FIG. 10. Normalized plot of the displacement $\bar{L}_1$ of the center of gravity of the core when an $n = 1$ modal disturbance of amplitude Δ is applied initially at the outer boundary of an undisturbed eddy with R_2 equal to $a = 2.5$, and with annular vorticity $= -2/5.25$. The (45°) straight line corresponds to linear theory [Eq. (3)]. The triangles are for $\Delta = 0.4$, the crosses are for $\Delta = 0.75$, and the dots are for $\Delta = 1$.

dipole moment in Fig. 10 are all for the same values of $n = 1$, $a = 2.5$, $w = -2/5.25$. This figure shows that the departure from (3) increases with time and with Δ.

Figure 8 also shows the same kind of intrusive filament as obtained previously (for $n = 2$). A similar intrusion (not shown) was found for an $n = 1$ disturbance with $\Delta = 0.75$. For $\Delta = 0.4$, wave breaking at the outer boundary occurred at $t = 18$, and the subsequent intrusive filament had a noticeably smaller area. At $t = 30$ another wave started to break at a position 90° clockwise from the first one, and a second small intrusion started to form.

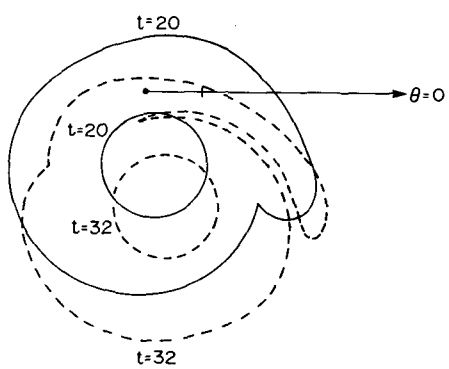

FIG. 11. The motion induced in a compact eddy ($a = 2.5$) by a cyclonic ($C = 0.5$) point vortex located at $\theta = 0$, $r = R = 7.5$ in the fixed polar coordinate system (the tick mark on the $\theta = 0$ axis denotes unit distance from the origin).

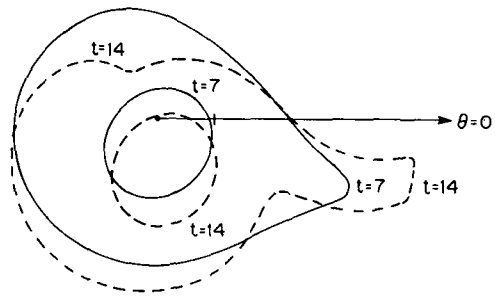

FIG. 12. As in Fig. 11 except R and C are decreased by half. The main effect at $t = 14$ is the commencement of a detrainment process.

5. Generating the disturbance

It is now necessary to discuss a mechanism for generating the initial disturbance on our robust ocean eddy, and the simplest way to begin is by placing a fixed point vortex having circulation C at a distance $R > a$ from an initially circularly symmetric eddy. Then the point vortex will distort the outer interface of the eddy, and the evolution can be computed by a small modification of the program used previously.

When $R = 7.5$, $C = 0.5$ (Fig. 11) the *inner* core is relatively undisturbed, and its center rotates about the fixed point at a rate expected by the R, C values. But larger distortions appear on the outer interface and these start to break at $t = 20$. At $t = 32$ a lobe of the eddy tends to be drawn towards the fixed point vortex and the filamentary intrusion winds into the center of the eddy. We also see another wave starting to break on the opposite side. When both R and C are decreased by half (Fig. 12), the velocity induced at the eddy center is unaltered, but the shear across the eddy is increased. This causes a more prominent lobe which seems to be on the verge of detrainment.

Reversing the sign of C (Fig. 13) changes the side of the eddy on which the lobe appears, and reduces the tendency for it to be drawn towards the fixed point. The predominant effect here appears to be engulfment or entrainment of the irrotational water mass.

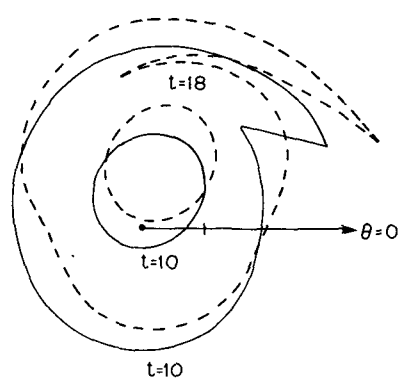

FIG. 13. As in Fig. 12 except that the sign of C is reversed.

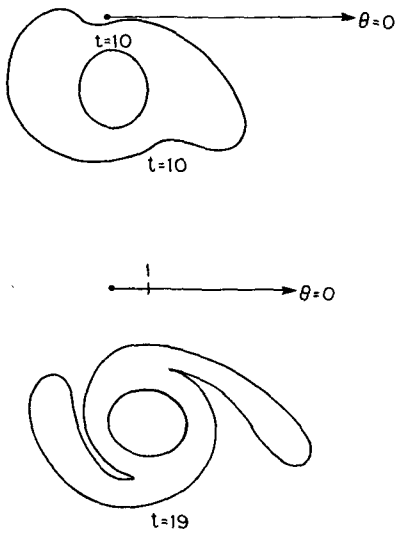

FIG. 14. As in Fig. 12 except that $C = 1.5$.

The value of R in Fig. 14 is the same as in Fig. 12, but the value of C has been tripled. The main effect on the eddy of the increased shear at $t = 10$ is the induction of an $n = 2$ mode. Two lobes develop after wave breaking [at $t = 16$ (not shown)], and at $t = 19$ we see two irrotational intrusions which almost pinch off two anticyclonic lobes. This calculation suggests how entrainment and detrainment can combine to lead to a more rapid isopycnal mixing of an eddy as its outer portion is replaced by the exterior water mass (Stern, 1987).

6. Conclusion

Shear instability in a compact barotropic eddy occurs when the annular width of the outer part (anticyclonic vorticity) becomes sufficiently small compared to the radius of the inner part (cyclonic vorticity). The nonlinear evolution causes the eddy to split into dipoles no matter how small the supercriticality of the basic state.

This paper mainly directs attention to the linearly stable eddy subjected to large displacements of the vorticity isopleths at its outer boundary. In this case the evolution of an $n = 2$ disturbance can cause a thin filament of the exterior water mass to penetrate into the eddy up to the radius of maximum azimuthal velocity, while maintaining the monopolar character of the streamfunction.

An azimuthal perturbation of wavenumber $n = 1$ causes a self-propagation of the entire eddy, also accompanied by wave breaking and filamentary intrusions at its outer boundary.

When a compact circularly symmetric eddy is perturbed by an exterior velocity field, breaking waves develop on the outer interface, and these lead to detraining filaments (Fig. 14) as well as intrusive ones.

This paper and its companion (Stern, 1987) suggest that similar effects should occur in isopycnal layers of a baroclinic eddy surrounded by a different water mass. In that case, the deformations of potential vorticity isopleths will produce isopycnal fluxes of the temperature/salinity anomalies. The straining of these structures produces strong *vertical* gradients of temperature and salinity on the fine- and microscales and these are associated with the final (thermodynamic) mixing of the temperature/salinity variances.

Acknowledgments. Thanks to Prof. G. Flierl for discussing some of this material with me at the 1986 Geophysical Fluid Dynamics Program at W.H.O.I., and thanks to ONR for partial financial support.

REFERENCES

Cheney, R. E., and P. L. Richardson, 1976: Observed decay of a cyclonic Gulf Stream ring. *Deep-Sea Res.*, **23**, 134–155.

Flierl, G., 1985: Instability of vortices. GFD Summer Program at the Woods Hole Oceanographic Institution, unpublished.

Gent, P. R., and J. C. McWilliams, 1986: The instability of barotropic circular vortices. *Geophys. Astrophys. Fluid Dyn.*, **35**, 209–233.

Ikeda, M., 1981: Instability and splitting of mesoscale rings using a two-layer quasi-geostrophic model on an *f*-plane. *J. Phys. Oceanogr.*, **11**, 987–998.

Joyce, T. M., 1984: Velocity and hydrographic structure of a Gulf Stream warm-core ring. *J. Phys. Oceanogr.*, **14**, 937–946.

——, R. W. Schmitt and M. C. Stalcup, 1983: Influence of the Gulf Stream upon the short-term evolution of a ring. *Aust. J. Mar. Freshwater Res.*, **34**, 515–524.

Lambert, R. B., 1984: Small-scale dissolved oxygen variations and the dynamics of Gulf Stream eddies. *Deep-Sea Res.*, **21**, 529–546.

Melander, M. V., E. A. Overman II and N. J. Zabusky, 1986: Computational vortex dynamics; in two and three dimensions. *Proc. Workshop on Numerical Fluid Dynamics*, North-Holland.

Overman, E. A., and N. J. Zabusky, 1982: Evolution and merger of isolated vortex structures. *Phys. Fluids*, **25**(8), 1297–1305.

Schmitt, R. W., R. G. Lueck and T. M. Joyce, 1986: Fine and microstructure at the edge of a warm core ring. *Deep-Sea Res.*, in press.

Stern, M. E., 1985: Lateral wave breaking and "shingle" formation in large-scale shear flow. *J. Phys. Oceanogr.*, **15**, 1274–1283.

——, 1987: Large-scale lateral entrainment and detrainment at the edge of a geostrophic shear layer. *J. Phys. Oceanogr.*, **17**, 1680–1687.